Scalable Deep Learning of Histology Images Reveals Genetic and Phenotypic Determinants of Adipocyte Hypertrophy

Emil Jørsboe[1,2,3,4], Phil Kubitz[5,6,7], Julius Honecker[5], Andrea Flaccus[8], Dagmar Mvondo[8], Matthias Raggi[9], Craig A. Glastonbury[10,11], Torben Hansen[3], Matthias Blüher[12,13], Aleksander Krag[4,14], Hans Hauner[5,15], Philip D. Charles[1,10,16,+], Cecilia M. Lindgren[1,2,6,+], Christoffer Nellåker[1,17,+], Melina Claussnitzer[6,7,18,+]

1. Big Data Institute, Li Ka Shing Centre for Health Information and Discovery, University of Oxford, Oxford, United Kingdom

2. Nuffield Department of Population Health, University of Oxford, Oxford, United Kingdom

3. Novo Nordisk Foundation Center for Basic Metabolic Research, Faculty of Health and Medical Sciences, University of Copenhagen, Copenhagen, Denmark

4. Center for Liver Research, Department of Gastroenterology and Hepatology, Odense University Hospital, Odense, Denmark

5. Technical University of Munich, Else Kröner-Fresenius-Center for Nutritional Medicine, Chair of Nutritional Medicine, School of Life Sciences, Gregor-Mendel-Straße 2, 85354, Freising-Weihenstephan, Germany

6. Broad Institute of MIT and Harvard, Medical and Population Genetics Program & Type 2 Diabetes Systems Genomics Initiative, Cambridge, MA, USA

7. Novo Nordisk Foundation Center for Genomic Mechanisms of Disease, Broad Institute of MIT and Harvard, Cambridge, MA, USA

8. Institute of Nutritional Sciences, University of Hohenheim, Stuttgart, Germany

9. Department of General and Visceral Surgery, Karl-Olga-Krankenhaus, Stuttgart, Germany

10. Nuffield Department of Medicine, University of Oxford; Oxford, United Kingdom

11. Human Technopole, Viale Rita Levi-Montalcini 1, 20157, Milan, Italy

12. Helmholtz Institute for Metabolic, Obesity and Vascular Research (HI-MAG) of the Helmholtz Zentrum München at the University of Leipzig and University Hospital Leipzig, Leipzig, Germany

13. Medical Department III - Endocrinology, Nephrology, Rheumatology, University of Leipzig Medical Center, Leipzig, Germany

14. Institute of Clinical Research, University of Southern Denmark, Odense, Denmark

15. Institute for Nutritional Medicine, School of Medicine and Health, Technical University of Munich, Georg-Brauchle-Ring 62, 80992, Munich, Germany

16. Target Discovery Institute, Centre for Medicines Discovery, Nuffield Department of Medicine, University of Oxford, Oxford, United Kingdom

17. Nuffield Department of Women's & Reproductive Health, University of Oxford, Oxford, United Kingdom

18. Diabetes Unit and Center for Genomic Medicine, Massachusetts General Hospital, Boston, MA, USA

Corresponding authors:

Christoffer Nellåker: christoffer.nellaker@wrh.ox.ac.uk, Melina Claussnitzer: melina@broadinstitute.org

+ = Shared senior authors

Abstract

Background: White adipose tissue dysfunction has emerged as a critical factor in cardiometabolic disease development, yet the cellular microstructure and genetic architecture of adipocyte morphology remain poorly explored.
Methods: We introduce Adipocyte U-Net 2.0, an advanced deep learning method for the semantic segmentation of adipose tissue histology, enabling analysis of over 27 million adipocytes from 2,667 individuals.
Findings: Our approach revealed that adipocyte hypertrophy associates with metabolic dysfunction, including increased fasting glucose, glycated hemoglobin, leptin, and triglycerides, with decreased adiponectin and HDL cholesterol levels. Through the largest genome-wide association study of adipocyte size to date ($N_{Subcutaneous}$ = 2,066, $N_{Visceral}$ = 1,878), we identified four genome-wide significant loci: two in sex-combined analysis (rs73184721 in *NAALADL2* and rs200047724 in *NRXN3*) and two female-specific variants (rs140503338 and rs11656704 in *ULK2*). Notably, these genetic associations showed congruent relationships with cardiometabolic traits, suggesting shared biological mechanisms.
Interpretation: Our findings demonstrate the utility of deep learning for adipocyte phenotyping at scale and provide novel insights into the genetic basis of adipocyte morphology and its relationship to metabolic disease.

Funding:

E.J and C.N. funded by an Alliance Grant from The Novo Nordisk Foundation Center for Basic Metabolic Research an independent research centre at the University of Copenhagen, partially funded by an unrestricted donation from the Novo Nordisk Foundation (NNF18CC0034900 and NNF23SA0084103). M.C. is the Weissman Davis and Titlebaum Family MGH Research Scholar Class 2024-2029 and M.C. as well as P.K. are supported by the Novo Nordisk Foundation (NNF21SA0072102). C.M.L. is supported by the Li Ka Shing Foundation, NIHR Oxford Biomedical Research Centre, Oxford, NIH (1P50HD104224-01), Gates Foundation (INV-024200), and a Wellcome Trust Investigator Award (221782/Z/20/Z) which also supports P.D.C.. H.H. and J.H. are funded by the Else Kröner Fresenius Foundation, Bad Homburg, Germany.

Introduction

Obesity is a rapidly growing global healthcare problem. Individuals with obesity are characterised by an increased cardiometabolic disease risk, including type 2 diabetes (T2D), coronary artery disease, and metabolic dysfunction–associated steatotic liver disease (1,2). Recent large-scale genome-wide association studies (GWAS) of body fat distribution, fasting insulin levels, and T2D highlight white adipose tissue (WAT) as a key tissue in which disease-associated variants manifest their effect (3).

During the development of obesity, WAT expands due to a combination of increasing adipocyte size (hypertrophy) and number of adipocytes (hyperplasia). While WAT expansion through hyperplasia is not associated with obesity-associated metabolic complications, hypertrophy is associated with ectopic fat accumulation in the liver, skeletal muscle, pancreas, and heart tissue, local inflammation (4), cardiometabolic risk (4), and impaired glucose metabolism (5). Expansion of white adipose tissue in adults is primarily characterised by hypertrophy (6). In individuals with obesity and adipocyte hypertrophy, the storage capacity of triglycerides is limited, and further caloric overload leads to fat accumulation in peripheral tissues and in visceral adipose depots (4). Enlargement of adipocytes is associated with low-grade chronic inflammation, insufficient angiogenesis, and excessive collagen deposition, which further leads to dysfunctional adipokine release (7). Adipocyte hypertrophy correlates strongly with insulin resistance and T2D in visceral adipose tissue, independently of body mass index (BMI) (8).

Obesity and fat distribution are highly heritable traits (9,10), and recent large-scale genetic association studies (11,12) have identified well over 1,000 independent genetic risk loci for fat mass and distribution-related traits. However, the disease-driving cellular processes remain largely unclear. We hypothesized that adipocyte hypertrophy is one such disease-driving phenotype. There is a lack of large-scale, well-powered GWAS mapping of the genetic determinants of adipocyte morphology (13,14), and the underlying genes and regulatory pathways involved in the size of adipocytes are not well characterised (15).

Historically, a practical limiting factor has been the lack of tools that allow for scalable and affordable mapping of adipocyte size. WAT histology samples can be used for studying adipocyte morphology (16), but manual annotation is cumbersome and extremely slow, and software for image-based measurements of adipocyte rarely scales well for practical application to large datasets. We previously developed Adipocyte U-Net, a deep learning approach for estimating the size of adipocytes across thousands of white adipose tissue histology samples (17). This model was validated against established methods, including Adiposoft (16) and CellProfiler (17), but analysis of contemporary data cohorts (N ~ 1,000) did not identify genome-wide significant genetic associations, likely due to limited statistical power, cohort heterogeneity, and limits on phenotypic resolution.

A limitation of our previous approach was the image-tiling strategy, which involved splitting whole slide images (WSIs) into sub-images and analyzing only tiles containing complete adipocytes. This methodology excluded adipocytes intersecting tile boundaries, which may bias size estimates downward since larger hypertrophic cells are more likely to intersect a boundary. Our previous U-net-based size estimates were consistently smaller compared to those from Adiposoft or CellProfiler (14).

To address this limitation and enable a comprehensive investigation of adipocyte morphology and its genetic determinants, we have developed an improved deep learning approach, Adipocyte U-Net 2.0, capable of accurately segmenting adipocytes across entire WSIs while properly accounting for cells that cross tile boundaries. Applying this enhanced methodology to an unprecedented collection of 9,000 WSIs containing over 27 million adipocytes from 2,667 individuals across five independent cohorts, we characterize the relationship between adipocyte hypertrophy and metabolic health, and perform the largest GWAS of adipocyte size to date, revealing novel genetic determinants of this clinically relevant cellular phenotype.

Methods

Training Adipocyte U-Net 2.0

We implemented Adipocyte U-Net 2.0 based on U-net (18) in PyTorch (19) for the semantic segmentation of adipocytes in WSIs. The model is based on the design in (17), with added dilations for the lowest resolution layer. The training, validation and hold-out test split was 70%, 15% and 15%, respectively.

The dice score of our validation with the lowest loss (0·36) was 0·83 (Supplementary Figure 1), the dice score of our held-out test set was 0·87.

Deep learning-derived phenotypes

For prediction, we adapted the code base for HAPPY (20), implemented in Python and using PyTorch for semantic segmentation. Tiles of 1024x1024 pixels are used, starting from the top left corner of the WSI and moving left to right in rows (Figure 1).

Segmentation is performed twice on each WSI, with a pixel size of 0·2500 µm and 0·5034 µm. The segmentation mask is efficiently stored as polygons, using the shapely library.

Post-Processing

The merged polygon list was filtered for area greater than 316·23 μm^2 and a Polsby-Popper (PP) roundness value (21) greater than 0·6 (empirically based distribution derived thresholds; prefiltered distributions and selected thresholds are shown in Supplementary Figure 2 & 3) (Figure 1A).

From the filtered polygons from each individual, we calculated mean adipocyte size and upper 95%-quantile of adipocyte size, and the ratio between mean adipocyte size in visceral and subcutaneous visceral adipose tissue.

For more technical details on the training of the model, derivation of phenotypes and post-processing see the Supplementary Methods.

Validation of Adipocyte U-Net 2.0-based estimates of adipocyte size against Adiposoft

Using WSIs from the Leipzig cohort, we ran Adiposoft on 10 tiles (1024x1024 pixels) per 17 WSIs. The WSIs were chosen randomly, and the tiles containing adipocytes were chosen. We used the same lower size cutoff of 316·23 μm^2 as for our Adipocyte U-net 2.0-based

approach and adipocytes at the edge of the tile were discarded, as Adiposoft only includes the area inside the tile for adipocytes at the edge.

For comparison with our Adipocyte U-net 2.0, we extracted the polygons within the coordinates of the tiles used with Adiposoft, we also removed polygons touching the edge of the tile to ensure consistent comparison.

Cohorts

WAT samples from subcutaneous and visceral depots were obtained from five different study cohorts (Table 1). Each study participant gave written informed consent and the protocols were approved by the corresponding ethics committee. Munich and Hohenheim: 5716/13, 1946/07, 409/16s. Leipzig: 159-12-21052012, 017-12-23012012. ENDOX: REC: 09/H0604/58, IRAS: 8282, GTEX: NIH (project id phs000424.v7.p2).

Cohort	Individuals with WSI (SC / VC)	Phenotypes	BMI (mean, SD)	Age (mean, SD)	Sex (M / F)
Munich	211 / 232	Anthropometric and metabolic	45·13, 12·58	46·13, 12·71	105 / 204
Leipzig	1151 / 1145	Anthropometric and metabolic	46·62, 11·49	49·77, 13·01	403 / 766
Hohenheim	47 / 50	Anthropometric and metabolic	46·55, 6·23	42·31, 13·09	37 / 114
Endox (Oxford)	425 / 55	Anthropometric	26·60, 5·80	32·78, 7·59	0 / 352
GTEX	918 / 759	Anthropometric and metabolic	27·32, 4·13	52·76, 12·91	653 / 327

Table 1. An overview of the five study cohorts used in this study and the number of WSIs per cohort. BMI, age and sex information is the number of individuals with phenotypes; these numbers might therefore differ from the number of individuals with WSIs.

Munich, Leipzig and Hohenheim cohorts

Male and female patients undergoing abdominal laparoscopic surgery were included. Subcutaneous adipose tissue biopsy derived from beneath the skin at the abdominal surgical incision site and visceral adipose tissue was obtained at the proximity of the angle of His. After sampling, approx. 5 mm^3 pieces of the tissue biopsies were sectioned and fixed in 4% paraformaldehyde for histology.

ENDOX cohort

Female premenopausal participants were recruited at the Oxford Endometriosis CaRe Centre between 2012 and 2018 for endometriosis screening via laparoscopy. Biopsies of the endometrium, peritoneal fluid, and adipose tissue from subcutaneous and visceral depots were obtained (17).

GTEX cohort

Whole slide images from HE stained subcutaneous and visceral adipose tissue samples were obtained from the Genotype Tissue and Expression (GTEX) project. Samples were obtained from individuals post-mortem. Subcutaneous adipose tissue biopsies were sampled at the leg, approx. 2 cm below the patella, and visceral adipose tissue was obtained from the omentum (22).

Histology and imaging
Dehydration and clearing of fixated histology samples were performed automatically (TP1020, Leica, Germany). Afterwards, samples were embedded in paraffin and 5 µm thick tissue sections were obtained using a rotary microtome (RM2255, Leica, Germany). Subsequently, the tissue sections were transferred to a glass microscope slide, hematoxylin and eosin (H&E) staining was applied using a fully automated multistainer (ST5020, Leica, Germany) and the samples were immediately coverslipped. Digital whole slide images were obtained using a slide scanner (Aperio AT2, Leica, Germany).

Genotyping
The Leipzig cohort was genotyped in two different batches. Lack of batch effect was confirmed via PCA with pruning and only with autosomal markers, filtering for MAF>0·05 and missingness<0·01 (Supplementary Figure 4). The two genotype files were merged into one file, which was used for all subsequent analyses.

For an overview of the genetic data and quality control, see respectively Supplementary Table 1 and Supplementary Methods.

Imputation
Each SNP-chip was phased and imputed independently after applying a quality control filter (see "Genetic Quality Control" section in Supplementary Methods), splitting by chromosome, and preparing the input files according to the TOPMed guidelines (https://topmedimpute.readthedocs.io/en/latest/). The TOPMed Imputation server was used (23). Eagle v2.4 (24) was used for phasing and Minimac4 (23) for imputation, both with the multiethnic TOPMed r2 reference panel, selecting the "vs. TOPMed panel" as the population.

Association analysis
GWAS was performed using bimbam mean genotype files, including genetic variants with an imputation Rsq > 0·3. A linear mixed model was run on each cohort using GEMMA (25). The model was adjusted for sex, age, age^2, sex·age, and the top ten genetic PCs. The ENDOX cohort was analysed jointly and the linear mixed model was additionally adjusted for which SNP-chip type. The Hohenheim cohort and part of the Munich cohort genotyped on the same SNP-chip were jointly analysed. The phenotypes were analysed raw and inverse normal quantile transformed. The outputs from each cohort were meta-analysed and the joint estimates of effect size and P-value were derived using the inverse variance-based strategy using METAL (26).

Furthermore, a phenome-wide association study (PheWAS) was performed for the lead variants using a meta-analysis-based approach. We focused on traits that were linked to hypertrophy, i.e. BMI, waist-hip ratio (WHR), plasma glycated hemoglobin, fasting plasma glucose, fasting plasma insulin, plasma 2-hour blood glucose, Interleukin 6, Adiponectin, type II diabetes status and C-reactive protein.

Colocalisation
Colocalisation between adipocyte-derived and other metabolic traits was assessed using a Bayesian statistical test with the coloc R-package (version 5.2.2) (27). Genomic regions were defined by windows of 1 Mb around suggestive and significant GWAS signals ($P < 10^{-5}$). Overlapping regions were merged. The minimal data required by coloc were used as

input: SNP IDs, positions, effect sizes, standard errors, data type (quantitative or case-control), MAF and sample sizes. To identify potential causal variants, 95% credible sets of variants based on their posterior inclusion probabilities were created. A posterior probability PPH4 (H4: associations with both traits due to a single causal variant) > 80% was considered sufficient for the identification of colocalisation.

We analysed all the traits listed in Figure 2.

Adipocyte hypertrophy in the Leipzig cohort

Phenotype associations with mean adipocyte size were tested using a linear model. Adipocyte size was divided by 1,000 to make the effect sizes more meaningful. The linear model was adjusted for age, sex, BMI and T2D:

$$y_i = \alpha_i + \beta_{i1} \cdot meanAdipocyte_i + \beta_{i2} \cdot age_i + \beta_{i3} \cdot sex_i + \beta_{i4} \cdot BMI_i + \beta_{i5} \cdot ifDiabetes_i + e_i$$

Details on estimating the effect of subcutaneous adipose tissue sampling location and adipocyte size epidemiology using linear mixed models are described in the Supplementary Methods.

Results

To facilitate large-scale analysis of adipocyte morphology, we developed Adipocyte U-Net 2.0, an advanced deep learning framework for the semantic segmentation of adipocytes in histological whole slide images (WSIs). Our improved methodology builds upon our previous work to implement a comprehensive approach to WSI analysis that eliminates potential size bias. Rather than processing discrete, non-overlapping image tiles independently, Adipocyte U-Net 2.0 performs semantic segmentation across entire WSIs using overlapping tiles, enabling accurate identification and measurement of all adipocytes, including those that cross tile boundaries (Figure 1A).

From the segmented adipocytes, we calculated five key phenotypes for subsequent analyses: mean adipocyte size, upper 95%-quantile of adipocyte size (as a proxy for hypertrophy), and the ratio between mean adipocyte size in visceral and subcutaneous adipose tissue. Through optimized parallelization, our method achieved unprecedented throughput with a runtime of one week, enabling the analysis of 9,000 WSIs containing over 27 million adipocytes from 2,667 individuals across five independent cohorts.

The Adipocyte U-net 2.0 improves the detection of hypertrophic adipocytes compared to previous models

We validated Adipocyte U-net 2.0 against both our previous model and the semi-automatic segmentation via Adiposoft (28). Adipocyte U-net 2.0-based estimates of mean adipocyte size were benchmarked against Adiposoft, showing strong agreement between methods with a linear correlation of R^2 = 0·76 (Figure 1C), confirming the accuracy of our deep learning approach. Comparing Adipocyte U-net 2.0 against our previous model, using identical filtering criteria, we observe a strong linear correlation comparing the adipocyte size estimates from both models ($R2_{subcutaneous}$ = 0·99, $R^2_{visceral}$ = 0·99) (Figure 1D). Importantly,

however, the current implementation of the Adipocyte U-net 2.0 results in consistently larger size estimates ($\beta_{subcutaneous}$ = 1·44, $\beta_{visceral}$ = 1·4). Additionally, the model enables the detection of very large adipocytes at the upper tail-end of the distribution (Figure 1B).
Our results demonstrate that Adipocyte U-Net 2.0 maintains the speed and accuracy advantages of our previous approach while addressing limitations in the detection of very large adipocytes.

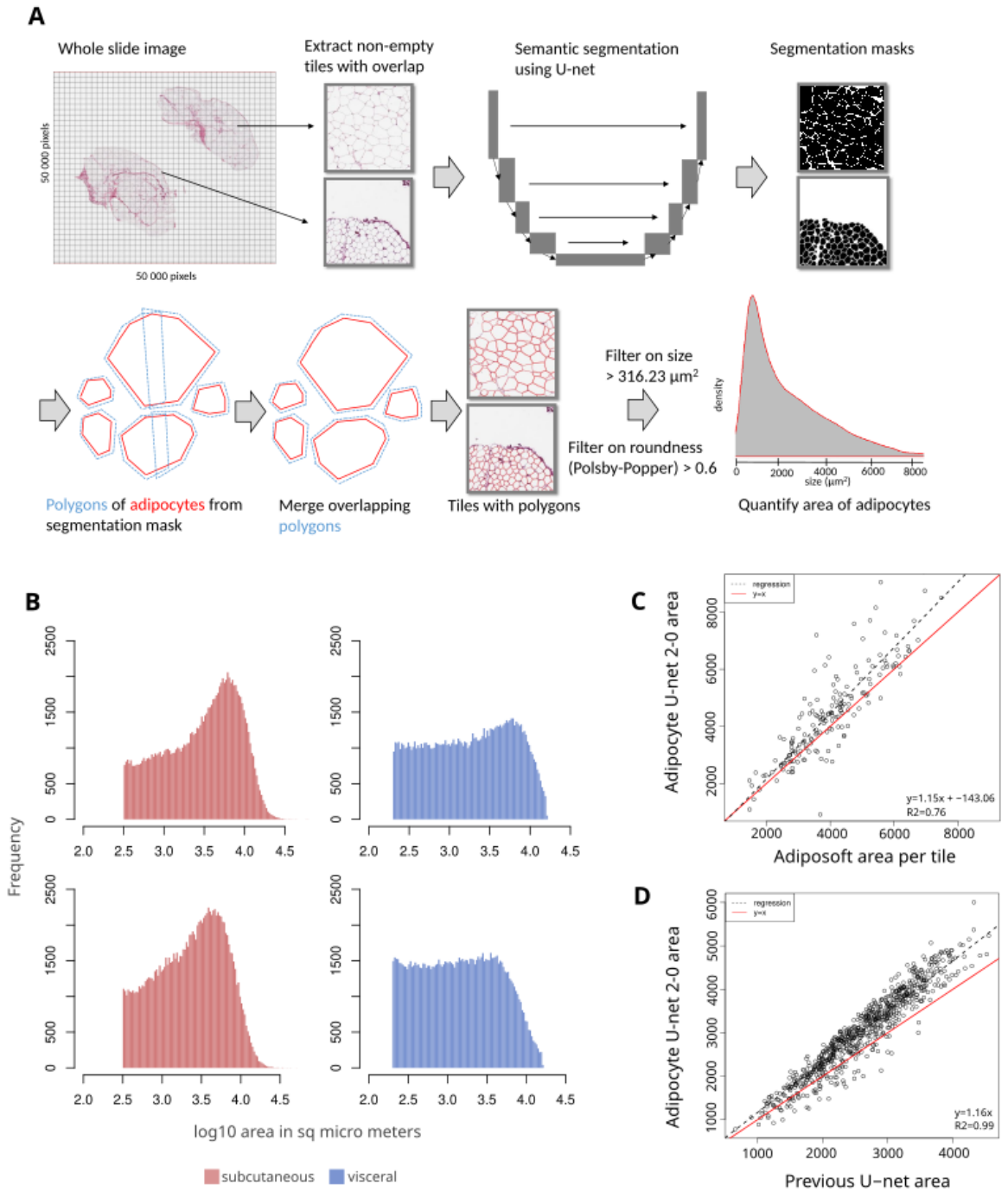

Figure 1. Adipocyte U-Net 2.0 captures adipocyte size-derived phenotypes from WSIs at scale. A) Workflow of adipocyte size quantification using Adipocyte U-net 2.0. **B)** 500

randomly sampled segmented adipocytes from WSIs from the Munich cohort using the filters from Adipocyte U-net 2.0 (upper histograms) using the filters (lower histograms) from (17). **C)** Comparison of mean adipocyte size estimates from Adipocyte U-net 2.0 and Adiposoft (28) based on 1024x1024 pixel tiles from the Leipzig cohort. **D)** Comparison of mean adipocyte size estimates from Adipocyte U-net 2.0 and (17) based on WSIs from the GTEX cohort.

Adipocyte hypertrophy is associated with demographic and metabolic status predominantly in visceral adipocytes

We set out to investigate the relationship between adipocyte size and a series of clinical variables across adipose tissue samples from 2215 visceral and 2527 subcutaneous donors with WSIs, encompassing 27 million adipocytes.

Mean adipocyte size increased with BMI in both the visceral depot ($\mu = 0{\cdot}39$, $P_\mu = 1{\cdot}89{\cdot}10^{-7}$, $\tau^2 = 0{\cdot}021$, $P_\tau = < 0{\cdot}0001$, $I^2 = 88{\cdot}5\%$) and the subcutaneous adipose depot ($\mu = 0{\cdot}40$, $P = 8{\cdot}28{\cdot}10^{-21}$, $\tau^2 = 0{\cdot}0057$, $P_\tau = 0{\cdot}0053$, $I^2 = 72{\cdot}8\%$) (Supplementary Figure 5-6). Mean adipocyte size also increased with age in the visceral adipose depot ($\mu = 0{\cdot}12$, $P_\mu = 0{\cdot}00014$, $\tau^2 = 0{\cdot}0020$, $P_\tau = 0{\cdot}09$, $I^2 = 51\%$), but not in subcutaneous ($\mu = 0{\cdot}07$, $P = 0{\cdot}15$, $\tau^2 = 0{\cdot}0068$, $P_\tau = 0{\cdot}0005$, $I^2 = 79{\cdot}9\%$) (Supplementary Figure 7-8). Stratifying by sex, mean adipocyte size was smaller in females compared to males in visceral adipose tissue ($\mu = -0{\cdot}32$, $P_\mu = 6{\cdot}77{\cdot}10^{-15}$, $\tau^2 = 0$, $P_\tau = 0{\cdot}49$), this sex-specificity of adipocyte size was not detected in the subcutaneous depots ($\mu = 0{\cdot}12$, $P_\mu = 0{\cdot}41$, $\tau^2 = 0{\cdot}061$, $P_\tau = < 0{\cdot}0001$, $I^2 = 91{\cdot}3\%$) (Supplementary Figure 9-10).

Comparing T2D cases to controls, we observed an increase in mean adipocyte size in the visceral depot ($\mu = 0{\cdot}11$, $P_\mu = 0{\cdot}021$, $\tau^2 = 0$, $P_\tau = 0{\cdot}69$) (Supplementary Figure 11-12). Mean visceral adipocyte size was significantly smaller compared to subcutaneous ($\mu = -0{\cdot}51$, $P = 1{\cdot}57{\cdot}10^{-7}$, $\tau^2 = 0{\cdot}037$, $P_\tau = < 0{\cdot}0001$, $I^2 = 86{\cdot}2\%$) (Supplementary Figure 13), replicating the finding from our previous study (14). This increase in subcutaneous adipocyte size is particularly evident in the GTEX cohort compared to all other cohorts collectively ($P_{ALL} = 3{\cdot}71{\cdot}10^{-35}$, $\beta_{ALL} = 771{\cdot}77$) and individually ($P_{Leipzig} = 2{\cdot}30{\cdot}10^{-23}$, $\beta_{Leipzig} = 773{\cdot}61$; $P_{Munich} = 1{\cdot}19{\cdot}10^{-9}$, $\beta_{Munich} = 728{\cdot}21$; $P_{Hohenheim} = 6{\cdot}97{\cdot}10^{-24}$, $\beta_{Hohenheim} = 2300{\cdot}19$; $P_{Endox} = 2{\cdot}93{\cdot}10^{-24}$, $\beta_{Endox} = 1004{\cdot}69$). Taken together, these results provide evidence that age, sex and T2D status are associated with visceral adipocyte hypertrophy.

Adipocyte hypertrophy is linked to clinical phenotypes in the context of cardiometabolic disease

To elucidate the relationship between adipocyte hypertrophy and cardiometabolic disease risk, we correlated mean adipocyte size measurements with relevant clinical biomarkers and adipokine levels utilizing data from the Leipzig cohort (Figure 2A-D).

Mean adipocyte size was positively correlated with levels of plasma glycated hemoglobin (mmol/mol) ($P_{SC} = 1{\cdot}06{\cdot}10^{-4}$, $\beta_{SC} = 2{\cdot}02$ and $P_{VC} = 1{\cdot}04{\cdot}10^{-3}$, $\beta_{VC} = 1{\cdot}93$) and with fasting plasma glucose in subcutaneous ($P_{SC_LOG10} = 3{\cdot}94{\cdot}10^{-5}$, $\beta_{SC_LOG10} = 0{\cdot}013$) and visceral adipose tissue ($P_{VC_LOG10} = 5{\cdot}06{\cdot}10^{-5}$, $\beta_{VC_LOG10} = 0{\cdot}015$). Furthermore, adiponectin was negatively ($P_{SC_LOG10} = 0{\cdot}011$, $\beta_{SC_LOG10} = -0{\cdot}045$, $P_{VC_LOG10} = 0{\cdot}017$, $\beta_{VC_LOG10} = -0{\cdot}052$) and leptin positively correlated with adipocyte size in both adipose depots ($P_{SC_LOG10} = 2{\cdot}03{\cdot}10^{-7}$, $\beta_{SC_LOG10} = 0{\cdot}042$, $P_{VC_LOG10} = 3{\cdot}19{\cdot}10^{-5}$, $\beta_{VC_LOG10} = 0{\cdot}042$). Lastly, the data revealed a positive association with interleukin 6 levels in visceral adipose tissue ($P_{VC_LOG10} = 0{\cdot}012$,

β_{VC_LOG10} = 0·14) (Figure 2A). These results are significant after controlling for FDR (Benjamini–Hochberg), (q-value = 0·036).

Next, we investigated the associations of adipocyte hypertrophy with blood lipid levels (Figure 2C-D). We found that mean adipocyte size correlated positively with levels of triglycerides (mmol/mol) ($P_{SC_LOG10} = 3{\cdot}53{\cdot}10^{-7}$, β_{SC_LOG10} = 0·032 and P_{VC_LOG10} = 0·013, β_{VC_LOG10} = 0·019), and the triglycerides to HDL cholesterol ratio ($P_{SC_LOG10} = 1{\cdot}32{\cdot}10^{-9}$, β_{SC_LOG10} = 0·049 and $P_{VC_LOG10} = 5{\cdot}15{\cdot}10^{-5}$, β_{VC_LOG10} = 0·039). We further observed a negative correlation with HDL cholesterol ($P_{SC} = 2{\cdot}97{\cdot}10^{-7}$, β_{SC} = -0·052 and $P_{VC} = 8{\cdot}28{\cdot}10^{-9}$, β_{VC} = -0·069) (Figure 2D). These results were significant after controlling for FDR (Benjamini–Hochberg), (q-value = 0·03). Interestingly, we observed no significant difference in levels of LDL cholesterol (P_{SC} = 0·38, β_{SC} = 0·027 and P_{VC} = 0·31, β_{VC} = 0·036) and total cholesterol (P_{SC} = 0·22, β_{SC} = 0·040 and P_{VC} = 0·96, β_{VC} = 0·0020).

Lastly, sex-stratified analyses revealed no statistically significant differences in effect sizes between males and females (Supplementary Figures 14-15).

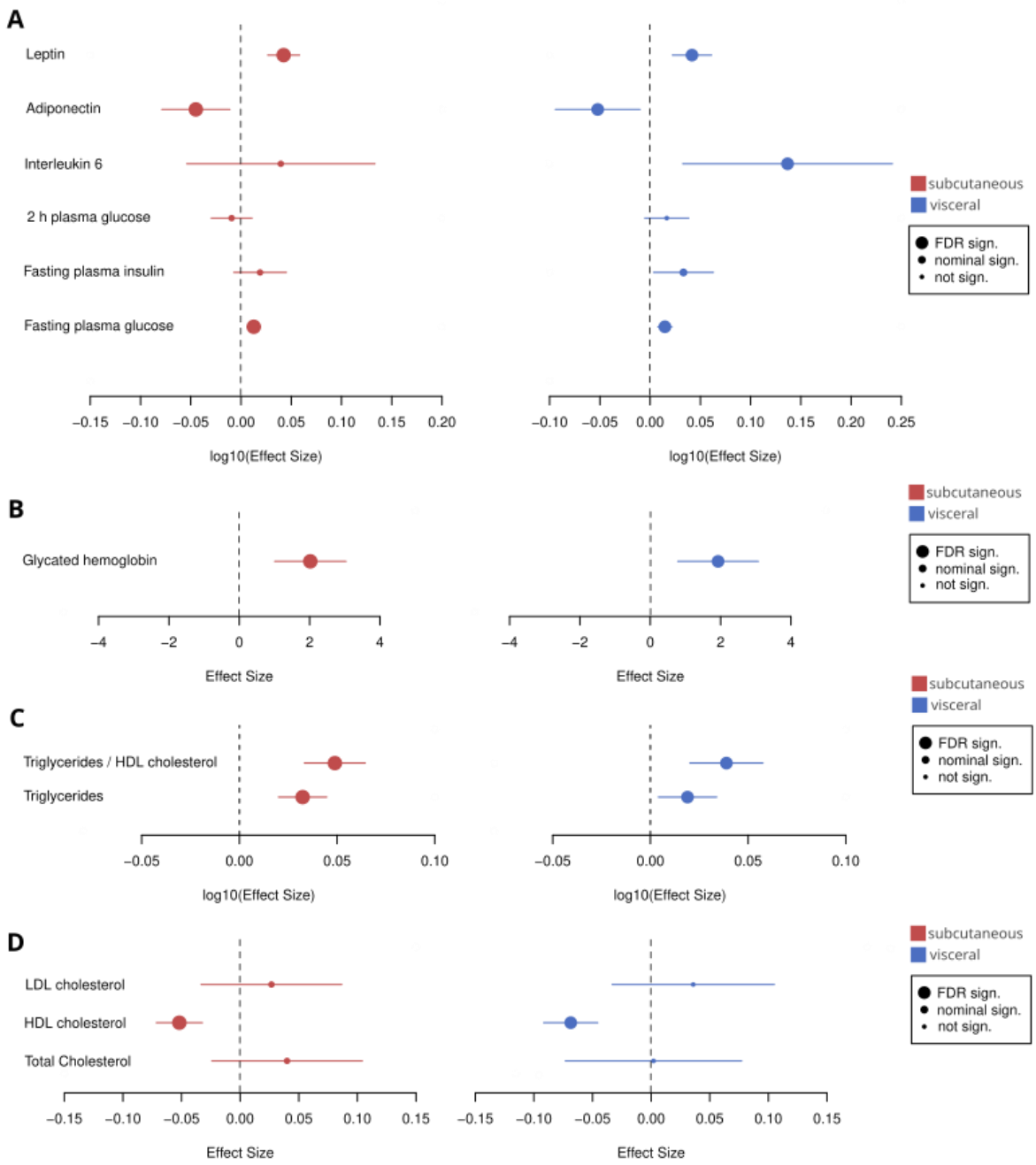

Figure 2. Effect size of mean adipocyte size on adipokine and glycemic traits **A)** and **B)** and lipid traits **C)** and **D)** with the 95% confidence intervals. q-values for the False Discovery Rate (FDR) are 0·036 for **A)** and **B)** and 0·03 for **C)** and **D)** respectively.

GWAS on adipocyte size reveals novel genetic associations with adipocyte hypertrophy

To identify genetic determinants of adipocyte size and adipocyte hypertrophy, we performed the largest sex-combined and sex-stratified GWAS of adipocyte morphology to date, analyzing five independent cohorts of European ancestry in both subcutaneous (N=2,066) and visceral (N=1,878) adipose tissues. Quantile-quantile plots showed no evidence of systematic inflation across our GWAS for all five adipocyte size phenotypes (Supplementary Figure 16). We identified four depot-dependent genetic signals reaching genome-wide

significance ($P < 5{\cdot}0{\cdot}10^{-8}$), represented by independent ($r2 < 0{\cdot}05$) index variants (Supplementary Figure 17).

Among the genome-wide significant loci, we detected an association for the intronic variant *rs73184721* (chr3:175280793, MAF=6·54% in EUR) in the *NAALADL2* gene with an increased 95%-quantile of adipocyte size in visceral adipose tissue ($\beta = 930{\cdot}18$, $\beta_{SD} = 0{\cdot}42$, $P = 7.01{\cdot}10^{-9}$) (Figure 3A). The association remained after adjusting for BMI ($\beta_{SD} = 0{\cdot}27$, $P = 1.19{\cdot}10^{-4}$) and did not show sex heterogeneity ($P = 0{\cdot}81$). Furthermore, the variant was also associated with increased mean adipocyte size in visceral adipose tissue ($\beta_{SD} = 0{\cdot}31$, $P = 3.87{\cdot}10^{-5}$).

Additionally, we detected an association between the small indel intronic variant *rs200047724* (chr14:78949603, MAF=2.14% in EUR), located in the *NRXN3* gene, and an increased 95%-quantile of adipocyte size in subcutaneous adipose tissue in our meta-analysis across all five cohorts ($\beta = 1592.92$, $\beta_{SD} = 0{\cdot}60$, $P = 6{\cdot}72{\cdot}10^{-8}$) (Figure 3B).

Sex-stratified analyses revealed genetic determinants specific to females (Supplementary Figure 18-19), but no genetic determinants specific to males (Supplementary Figure 20-21). We identified an association between the intergenic variant *rs140503338* (chr14:68826371, MAF=2.15% in EUR) and increased mean adipocyte size exclusively in females in subcutaneous adipose tissue meta-analyzing all five cohorts ($\beta = 956{\cdot}06$, $\beta_{SD} = 0{\cdot}85$, $P = 2.70{\cdot}10^{-8}$) (Supplementary Figure 22). This variant was also associated with an increased 95%-quantile of adipocyte size in females in subcutaneous adipose tissue ($\beta_{SD} = 0{\cdot}78$, $P = 2.86{\cdot}10^{-7}$) and remained significant after adjusting for BMI ($\beta_{SD} = 0{\cdot}66$, $P = 4{\cdot}78{\cdot}10^{-6}$). While the genetic association of *rs14053338* with adipocyte size and hypertrophy in females was specific to subcutaneous adipose tissue, we observed a nominal association in the meta-analysis for mean visceral adipocyte size ($\beta_{SD} = 0{\cdot}32$, $P = 0{\cdot}044$) and 95%-quantile of visceral adipocyte size ($\beta_{SD} = 0{\cdot}35$, $P = 0{\cdot}028$) in females.
Finally, we identified an association between the intronic variant *rs11656704* (chr17:19789496, MAF=22.0%) in the *ULK2* gene with a decreased 95%-quantile of visceral adipocyte size in females ($\beta = -700{\cdot}64$, $\beta_{SD} = -0{\cdot}31$, $P = 4{\cdot}50{\cdot}10^{-8}$). This signal remained significant after adjusting for BMI ($\beta_{SD} = -0{\cdot}26$, $P = 7.36{\cdot}10^{-7}$) and mean adipocyte size ($\beta_{SD} = -0{\cdot}29$, $P = 4{\cdot}62{\cdot}10^{-7}$).

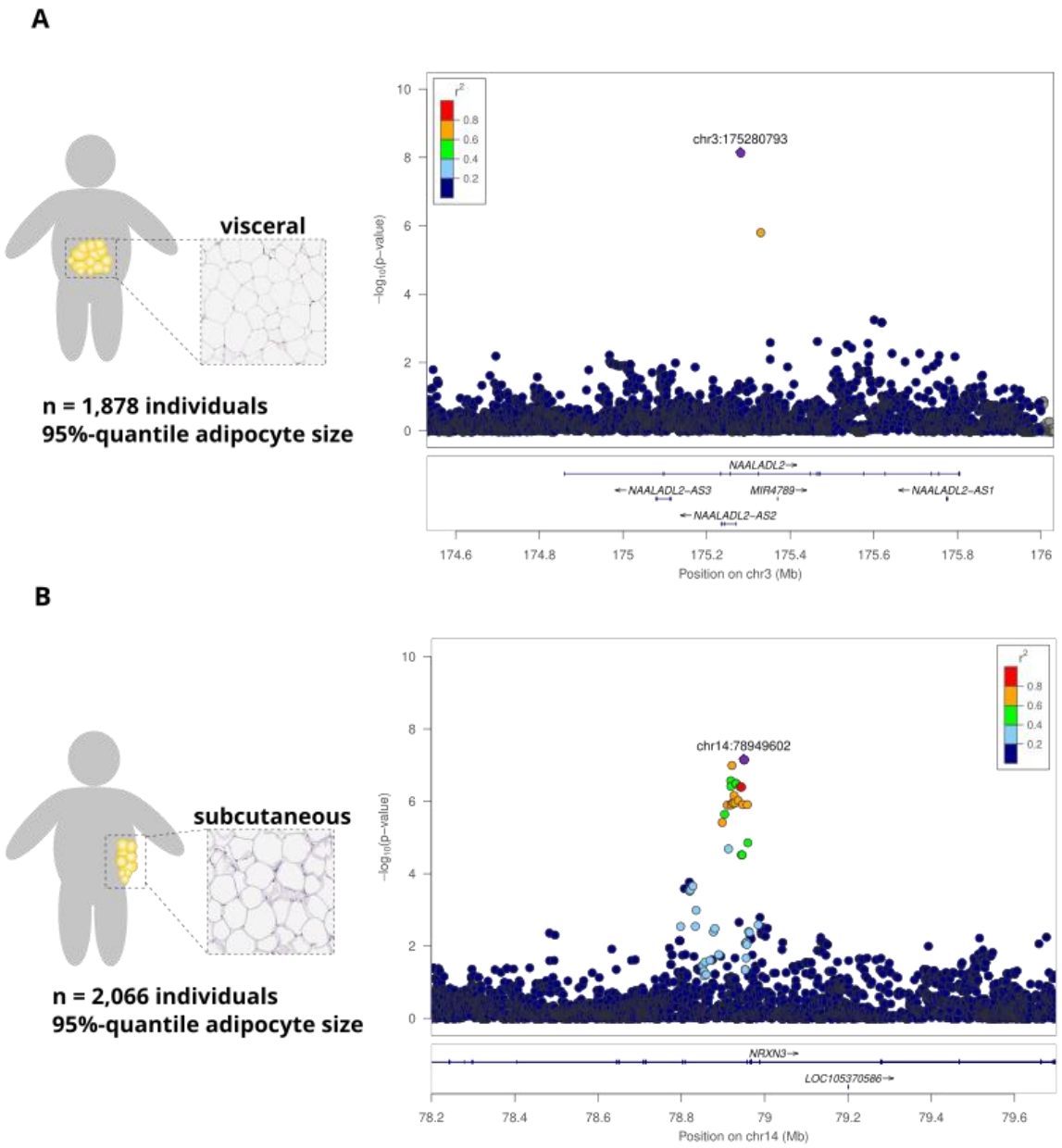

Figure 3. A) LocusZoom plot of rs73184721 (chr3:175280793) and its association with the 95%-quantile of adipocyte size in visceral adipose tissue. **B)** LocusZoom plot of rs200047724 (chr14:78949602) and its association with the 95%-quantile of adipocyte size in subcutaneous adipose tissue. For both plots, a region of +/- 750 kb has been plotted around the variant. The colour of the dots indicates the degree of LD between the lead variant and the other variants, the R2 values are based on the GTEX sequence data.

To evaluate the clinical relevance of these genetic associations in the context of metabolic disease, we performed phenome-wide association studies (PheWAS). Interestingly, the female-specific variant *rs14053338* was significantly associated with plasma glycated hemoglobin levels (β_{SD} = 0·65, P = 0·0081) (Table 2) and nominally associated with BMI (β_{SD} = 0·42, P = 0·016) and 2-hour plasma glucose (β_{SD} = 1.25, P = 0·046). The other female-

specific variant in *ULK2* was associated with WHR (β_{SD} = -0·54, P = 0·0056) and plasma glycated hemoglobin levels (β_{SD} = -0·26, P = 0·0055) in our PheWAS (Table 2).

Trait	rs73184721 (chr3) (P / βSD)	rs200047724 (chr14) (P / βSD)	rs140503338 (chr14) (P / βSD) (Females only)	rs11656704 (chr17) (P / βSD) (Females only)
WHR	**0·012 / -0·39**	0·054 / -0·58	0·27 / 0·58	**0·0056 / -0·54**
BMI	0·70 / -0·027	0·12 / -0·16	**0·016 / 0·42**	0·27 / -0·075
plasma glycated hemoglobin (%)	0·58 / 0·070	0·057 / -0·34	**0·0081 / 0·65**	**0·0055 / -0·26**
fasting plasma glucose	0·30 / -0·11	0·72 / -0·056	0·062 / 0·38	0·060 / -0·14
2h plasma glucose	0·95 / 0·020	0·063 / 1.05	**0·046 / 1.25**	0·60 / -0·15
fasting plasma insulin	0·41 / -0·12	0·49 / -0·18	0·35 / 0·27	0·16 / -0·15
Interleukin-6	0·88 / -0·066	0·59 / 0·28	0·89 / -0·072	0·32 / -0·21
Adiponectin	0·79 / -0·10	0·84 / -0·11	0·071 / -1.16	0·12 / 0·40
C-reactive protein	0·62 / -0·050	0·94 / 0·012	0·17 / 0·26	0·52 / -0·048

Table 2. PheWAS results for the three lead variants. P-value and effect size from the inverse normal quantile transformed traits are reported. These analyses are run in the Leipzig Cohort. All values with a P-value below 0·05 (nominal significance) have been highlighted in bold.

Discussion

Our novel approach of WSI segmentation enables comprehensive detection and quantification of adipocytes, including very large hypertrophic cells missed by previous methods. Our approach allows us to better characterize the metabolic impact of adipocyte hypertrophy and to investigate its genetic architecture at an unprecedented scale.

We show that increased adipocyte size is associated with an adverse metabolic profile, consistent with previously reported elevated risk of type 2 diabetes and increased plasma fasting glucose (8). This relationship with fasting plasma glucose appears stronger in visceral compared to subcutaneous adipose tissue ($\beta_{SC_LOG10} = 0{\cdot}013$ and $\beta_{VC_LOG10} = 0{\cdot}015$), in line with the established metabolic significance of visceral adiposity (8). The positive correlation between adipocyte size and levels of glycated hemoglobin corroborates findings from Keshavjee *et al.(29)*, who reported that increased average adipose cell area in visceral adipose tissue was associated with persistently elevated glycated hemoglobin following bariatric surgery (post-Roux-en-Y gastric bypass).

The inverse relationship between adiponectin levels and mean adipocyte size is consistent with previous findings (8). Interestingly, we detected a significant association between interleukin-6 and mean adipocyte size specifically in visceral but not in subcutaneous adipose tissue. This is inconsistent with (30), where levels of interleukin 6 were higher in diabetic and non-diabetic obese patients compared to control subjects in subcutaneous adipose tissue (Figure 2). The increased mean size of adipocytes in men and with increased age in visceral adipose tissue is consistent with the meta-analysis in (8). However, the finding of no increase in the mean size of adipocytes with age in subcutaneous adipose tissue is not. Additionally, the decreased mean adipocyte size in visceral depots is also consistent with the literature (8) (Supplementary Figure 5-13). Importantly, these results demonstrate significant heterogeneity between cohorts, suggesting that the surgery approach, anatomical location of the biopsy site and the study population characteristics are potential modifiers of adipocyte size.

Notably, we did not detect a statistically significant increase in fasting plasma insulin levels with an increased mean size of adipocytes, contrary to previous findings (8) (Figure 2). We also observed no sex-specific differences in the metabolic impact of adipocyte hypertrophy. (Supplementary Figure 14-15).

Our study represents a substantial advance in understanding the genetic architecture of adipocyte morphology. Only two previous studies, including our earlier work, have investigated this area (14,17), both failing to identify genome-wide significant associations ($P < 5.0{\cdot}10^{-8}$). We report four novel genetic loci associated with adipocyte size phenotypes. The variant rs73184721 is an intronic variant in the large *NAALADL2* gene, whose function remains largely unknown. However, another gene close to the associated variant is *NLGN1*, which acts as a splice site-specific ligand for β-neurexins. Intriguingly, this variant has been nominally associated with increased pancreas fat percentage and increased subcutaneous adipose tissue volume (31). *NLGN1* has also been linked to predicted visceral adipose tissue mass (12), BMI (32), and type 2 diabetes (33), suggesting that the effect on visceral adipocyte hypertrophy might be mediated through *NLGN1* expression, though this merits further investigation.

The association of rs200047724 in the *NRXN3* gene with the increased 95%-quantile of adipocyte size is particularly intriguing. *NRXN3*, neurexin 3, encodes proteins functioning as receptors and cell adhesion molecules primarily expressed in the brain. Intriguingly, the *NRXN3* gene has previously been associated with BMI (34), waist circumference (35), and altered methylation expression in extremely obese individuals (36), suggesting a neuronal component in the regulation of adipocyte morphology.

The female-specific variant rs140503338 is located near a gene cluster containing *RAD51B,* a member of the *RAD51* protein family essential for DNA repair by homologous recombination. This gene has been previously associated with waist-hip ratio (both BMI-adjusted (37) and unadjusted (38), and is most highly expressed in the uterus, potentially explaining its sex-specific effects (39). We therefore speculate that the observed association with adipocyte size might be mediated through the *RAD51B* gene, though this requires further investigation.

The other female-specific variant, rs11656704, is an intronic variant in the gene *ULK2* located near *AKAP10,* which has been previously associated with BMI (40). While this variant showed no association with BMI in our analysis, it was significantly associated with decreased waist-hip ratio and reduced plasma glycated hemoglobin levels (Table 2). This suggests that *AKAP10* may influence adipocyte morphology through mechanisms independent of overall adiposity, though this is speculative and the involvement of *AKAP10* as a causal effector in adipocyte morphology warrants further investigation.

Given the unusual linkage disequilibrium patterns observed for rs73184721 and rs140503338, we verified these patterns against both the 1000 Genomes (43) and TOPMed (44) reference panels, confirming their validity (41).

Interestingly, our colocalisation analysis revealed shared genetic architecture between adipocyte size and HDL cholesterol levels, with effects in the same direction as observed in our epidemiological analyses—increased visceral adipocyte size corresponded with decreased HDL cholesterol (Figure 2D). While the top variant (rs2070512) is an expression quantitative trait locus (eQTL) for *CCDC116* in both adipose depots and for *UBE2L3* and *YDJC* in subcutaneous adipose tissue, none of these genes have established connections to adipose biology, suggesting potential novel pathways linking adipocyte morphology to lipid metabolism.

To our knowledge, this study is the first to report genome-wide significant genetic associations with adipocyte size, providing important insights into the genetic architecture underlying this cellular phenotype. The identification of both sex-combined and female-specific loci offers intriguing insights into the sexual dimorphism of fat distribution and metabolic risk, a phenomenon long observed clinically but poorly understood mechanistically.

Intriguingly, two of our significant loci point toward a potential brain-adipose signaling axis. The association of *NRXN3* with subcutaneous adipocyte morphology suggests a connection between neuronal signaling and peripheral adipocyte behavior. Similarly, the proximity of *NLGN1* to our lead variant rs73184721 further strengthens this hypothesis, as neuroligins and neurexins form transynaptic complexes crucial for synaptic function. This convergence

of neuronal adhesion molecules in adipocyte size regulation suggests previously unexplored central nervous system influences on adipocyte biology, potentially coordinating energy homeostasis between brain and adipose tissue.

We stress that due to the lack of comparable genetic studies in this field, direct replication of our findings is currently not possible. However, as computational methods continue to advance, the combination of genetic data with deep learning-based histological analysis will likely yield further insights into the cellular foundations of metabolic disease and provide further validation. Our findings highlight the adipocyte as a genetically regulated and responsive cell type whose morphological characteristics play an important role in the link between obesity and metabolic complications.

Availability and implementation

The method is implemented in Python, making use of the PyTorch library. The code for training the model can be found at https://github.com/Nellaker-group/PyTorchUnet, and the code for running predictions with the model can be found here https://github.com/Nellaker-group/UNetHAPPY.

Acknowledgments

We would like to thank the Core Facility for Comparative Experimental Pathology at Klinikum Rechts der Isar, Technical University of Munich for their technical support in obtaining the whole slide images.

Author contributions

E.J., P.K., J.H., C.N., C.M.L., H.H. and M.C. conceived the study and designed the experiments. E.J., P.D.C. and C.N. wrote the code. E.J. and J.H. created ground truth annotations. E.J. performed the experimental analysis. J.H. and P.K. prepared and processed the adipose tissue histology samples. H.H., M.B., M.R, A.F., D.M, P.K. and M.C. collected the adipose tissue biopsies. E.J. conducted the genetic association studies of adipocyte morphology with input from T.H. and A.K. E.J. performed the quality control and imputation of the genetic data. E.J. and P.K. conducted the epidemiological studies of adipocyte morphology with input from P.D.C., C.N., and M.C.. E.J. and P.K. prepared the manuscript with input, revisions, and approval from M.C., C.A.G., H.H., M.B., T.H., C.M.L. and A.K. The supervision of the research was done by P.D.C., C.M.L., C.N., H.H. and M.C.

1. Zheng Y, Ley SH, Hu FB. Global aetiology and epidemiology of type 2 diabetes mellitus and its complications. Nat Rev Endocrinol. 2018 Feb;14(2):88–98.

2. Vernon G, Baranova A, Younossi ZM. Systematic review: the epidemiology and natural history of non-alcoholic fatty liver disease and non-alcoholic steatohepatitis in adults. Aliment Pharmacol Ther. 2011 Aug;34(3):274–85.

3. Lotta LA, Gulati P, Day FR, Payne F, Ongen H, Van De Bunt M, et al. Integrative genomic analysis implicates limited peripheral adipose storage capacity in the pathogenesis of human insulin resistance. 2017;49(1):17.

4. Longo M, Zatterale F, Naderi J, Parrillo L, Formisano P, Raciti GA, et al. Adipose Tissue Dysfunction as Determinant of Obesity-Associated Metabolic Complications. Int J Mol

Sci [Internet]. 2019 May 13;20(9). Available from: http://dx.doi.org/10.3390/ijms20092358

5. Gao H, Mejhert N, Fretz JA, Arner E, Lorente-Cebrián S, Ehrlund A, et al. Early B cell factor 1 regulates adipocyte morphology and lipolysis in white adipose tissue. Cell Metab. 2014 Jun 3;19(6):981–92.

6. Spalding KL, Arner E, Westermark PO, Bernard S, Buchholz BA, Bergmann O, et al. Dynamics of fat cell turnover in humans. Nature. 2008 Jun 5;453(7196):783–7.

7. Liu F, He J, Wang H, Zhu D, Bi Y. Adipose morphology: A critical factor in regulation of human metabolic diseases and adipose tissue dysfunction. Obes Surg. 2020 Dec 6;30(12):5086–100.

8. Ye RZ, Richard G, Gévry N, Tchernof A, Carpentier AC. Fat cell size: Measurement methods, pathophysiological origins, and relationships with metabolic dysregulations. Endocr Rev. 2022 Jan 12;43(1):35–60.

9. Bouchard C, Despres JP, Mauriege P. Genetic and nongenetic determinants of regional fat distribution. Endocr Rev. 1993 Feb;14(1):72–93.

10. Herrera BM, Lindgren CM. The genetics of obesity. Curr Diab Rep. 2010 Dec;10(6):498–505.

11. Pulit SL, Stoneman C, Morris AP, Wood AR, Glastonbury CA, Tyrrell J, et al. Meta-analysis of genome-wide association studies for body fat distribution in 694 649 individuals of European ancestry. Hum Mol Genet. 2019 Jan 1;28(1):166–74.

12. Karlsson T, Rask-Andersen M, Pan G, Höglund J, Wadelius C, Ek WE, et al. Contribution of genetics to visceral adiposity and its relation to cardiovascular and metabolic disease. Nat Med. 2019 Sep;25(9):1390–5.

13. Kulyté A, Aman A, Strawbridge RJ, Arner P, Dahlman IA. Genome-wide association study identifies genetic loci associated with fat cell number and overlap with genetic risk loci for type 2 diabetes. Diabetes. 2022 Jun 1;71(6):1350–62.

14. Lundbäck V, Kulyté A, Arner P, Strawbridge RJ, Dahlman I. Genome-wide association study of diabetogenic adipose morphology in the GENetics of Adipocyte Lipolysis (GENiAL) cohort. Cells. 2020 Apr 27;9(5):1085.

15. Glastonbury CA, Couto Alves A, El-Sayed Moustafa JS, Small KS. Cell-type heterogeneity in adipose tissue is associated with complex traits and reveals disease-relevant cell-specific eQTLs. Am J Hum Genet. 2019 Jun 6;104(6):1013–24.

16. The morphology of adipose tissue. In: New Perspectives in Adipose Tissue. Butterworth-Heinemann; 1985. p. 23–43.

17. Glastonbury CA, Pulit SL, Honecker J, Censin JC, Laber S, Yaghootkar H, et al. Machine Learning based histology phenotyping to investigate the epidemiologic and genetic basis of adipocyte morphology and cardiometabolic traits. PLoS Comput Biol. 2020 Aug;16(8):e1008044.

18. Ronneberger O, Fischer P, Brox T. U-net: Convolutional networks for biomedical image segmentation. Springer; 2015. 234-241 p. (International Conference on Medical image computing and computer-assisted intervention).

19. Paszke A, Gross S, Massa F, Lerer A, Bradbury J, Chanan G, et al. PyTorch: An

Imperative Style, High-Performance Deep Learning Library [Internet]. arXiv [cs.LG]. 2019. Available from: http://arxiv.org/abs/1912.01703

20. Vanea C, Džigurski J, Rukins V, Dodi O, Siigur S, Salumäe L, et al. HAPPY: A deep learning pipeline for mapping cell-to-tissue graphs across placenta histology whole slide images [Internet]. bioRxiv. 2023 [cited 2024 Mar 13]. p. 2022.11.21.517353. Available from: https://www.biorxiv.org/content/biorxiv/early/2023/02/27/2022.11.21.517353

21. Polsby D, Popper R. The Third Criterion: Compactness as a Procedural Safeguard Against Partisan Gerrymandering. 2015 Oct 16 [cited 2024 Mar 18]; Available from: https://digitalcommons.law.yale.edu/ylpr/vol9/iss2/6

22. Lonsdale J, Thomas J, Salvatore M, Phillips R, Lo E, Shad S, et al. The genotype-tissue expression (GTEx) project. 2013;45(6):580.

23. Das S, Forer L, Schönherr S, Sidore C, Locke AE, Kwong A, et al. Next-generation genotype imputation service and methods. Nat Genet. 2016 Oct;48(10):1284–7.

24. Loh PR, Danecek P, Palamara PF, Fuchsberger C, A Reshef Y, K Finucane H, et al. Reference-based phasing using the Haplotype Reference Consortium panel. Nat Genet. 2016 Nov;48(11):1443–8.

25. Zhou X, Stephens M. Genome-wide efficient mixed-model analysis for association studies. Nat Genet. 2012 Jun 17;44(7):821–4.

26. Willer CJ, Li Y, Abecasis GR. METAL: fast and efficient meta-analysis of genomewide association scans. Bioinformatics. 2010 Sep 1;26(17):2190–1.

27. Giambartolomei C, Vukcevic D, Schadt EE, Franke L, Hingorani AD, Wallace C, et al. Bayesian test for colocalisation between pairs of genetic association studies using summary statistics. PLoS Genet. 2014 May 15;10(5):e1004383.

28. Galarraga M, Campión J, Muñoz-Barrutia A, Boqué N, Moreno H, Martínez JA, et al. Adiposoft: automated software for the analysis of white adipose tissue cellularity in histological sections. J Lipid Res. 2012 Dec;53(12):2791–6.

29. Keshavjee SH, Schwenger KJP, Yadav J, Pickel L, Ghorbani Y, Sung HK, et al. Adipose tissue and plasma markers associated with HbA1c pre- and post-bariatric surgery: A cross-sectional and cohort study. Obes Surg. 2023 Aug 28;33(8):2443–51.

30. Bahceci M, Gokalp D, Bahceci S, Tuzcu A, Atmaca S, Arikan S. The correlation between adiposity and adiponectin, tumor necrosis factor alpha, interleukin-6 and high sensitivity C-reactive protein levels. Is adipocyte size associated with inflammation in adults? J Endocrinol Invest. 2007 Mar;30(3):210–4.

31. Liu Y, Basty N, Whitcher B, Bell JD, Sorokin EP, van Bruggen N, et al. Genetic architecture of 11 organ traits derived from abdominal MRI using deep learning. Elife [Internet]. 2021 Jun 15 [cited 2024 Sep 5];10. Available from: https://elifesciences.org/articles/65554

32. Huang J, Huffman JE, Huang Y, Do Valle Í, Assimes TL, Raghavan S, et al. Genomics and phenomics of body mass index reveals a complex disease network. Nat Commun. 2022 Dec 29;13(1):7973.

33. Vujkovic M, Keaton JM, Lynch JA, Miller DR, Zhou J, Tcheandjieu C, et al. Discovery of 318 new risk loci for type 2 diabetes and related vascular outcomes among 1.4 million

participants in a multi-ancestry meta-analysis. Nat Genet. 2020 Jul;52(7):680–91.

34. Locke AE, Kahali B, Berndt SI, Justice AE, Pers TH, Day FR, et al. Genetic studies of body mass index yield new insights for obesity biology. Nature. 2015 Feb 12;518(7538):197–206.

35. Heard-Costa NL, Zillikens MC, Monda KL, Johansson A, Harris TB, Fu M, et al. NRXN3 is a novel locus for waist circumference: a genome-wide association study from the CHARGE Consortium. PLoS Genet. 2009 Jun;5(6):e1000539.

36. McAllan L, Baranasic D, Villicaña S, Brown S, Zhang W, Lehne B, et al. Integrative genomic analyses in adipocytes implicate DNA methylation in human obesity and diabetes. Nat Commun. 2023 May 15;14(1):2784.

37. Lotta LA, Wittemans LBL, Zuber V, Stewart ID, Sharp SJ, Luan J ’an, et al. Association of Genetic Variants Related to Gluteofemoral vs Abdominal Fat Distribution With Type 2 Diabetes, Coronary Disease, and Cardiovascular Risk Factors. JAMA. 2018 Dec 25;320(24):2553–63.

38. Sieh W, Rothstein JH, Klein RJ, Alexeeff SE, Sakoda LC, Jorgenson E, et al. Identification of 31 loci for mammographic density phenotypes and their associations with breast cancer risk. Nat Commun. 2020 Oct 9;11(1):5116.

39. GTEx Consortium. The GTEx Consortium atlas of genetic regulatory effects across human tissues. Science. 2020 Sep 11;369(6509):1318–30.

40. Turcot V, Lu Y, Highland HM, Schurmann C, Justice AE, Fine RS, et al. Protein-altering variants associated with body mass index implicate pathways that control energy intake and expenditure in obesity. Nat Genet. 2018 Jan;50(1):26–41.

41. 1000 Genomes Project Consortium, Auton A, Brooks LD, Durbin RM, Garrison EP, Kang HM, et al. A global reference for human genetic variation. Nature. 2015 Oct 1;526(7571):68–74.

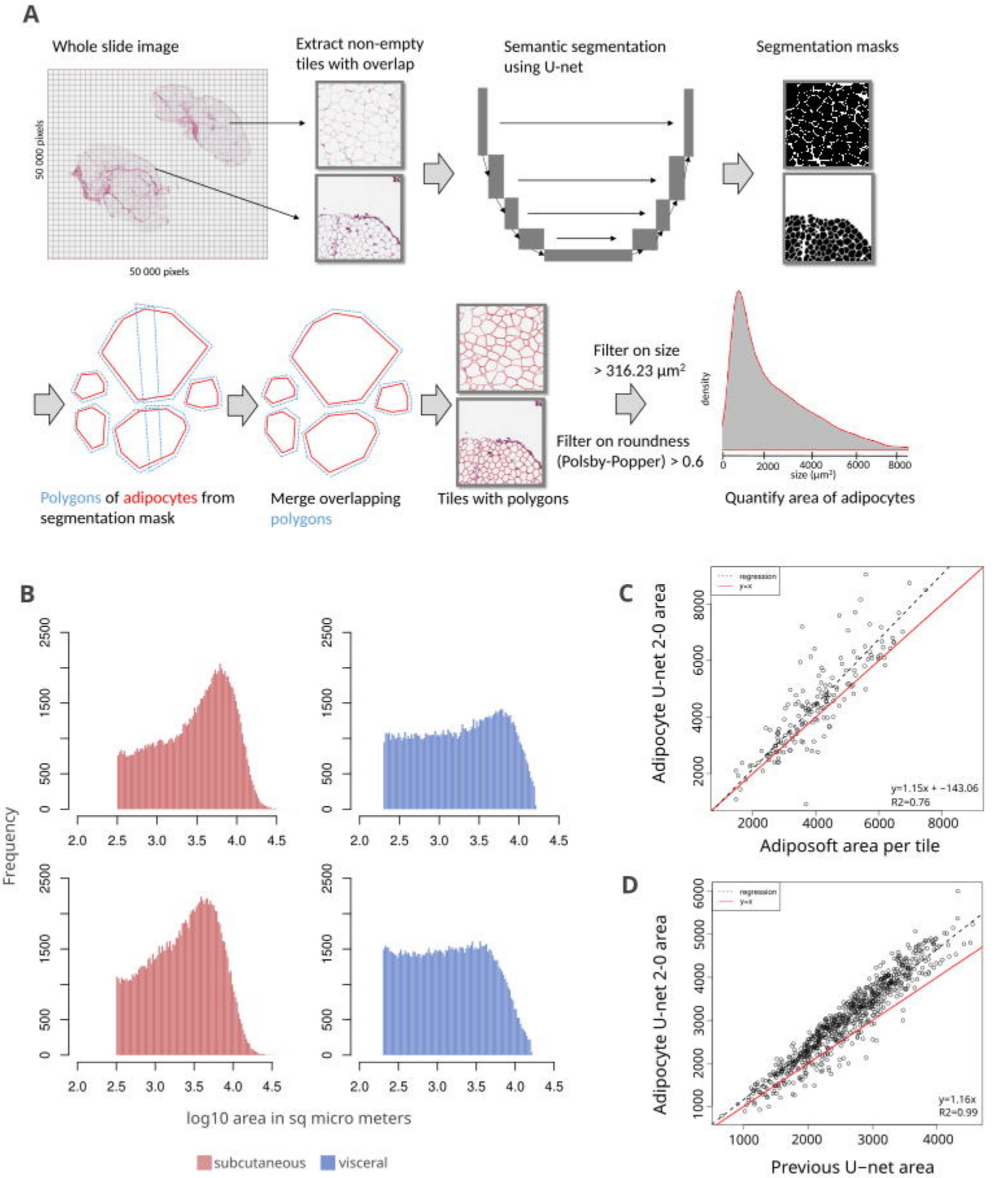
A
Whole slide image
50 000 pixels
50 000 pixels
Extract non-empty tiles with overlap
Semantic segmentation using U-net
Segmentation masks
Polygons of adipocytes from segmentation mask
Merge overlapping polygons
Tiles with polygons
Filter on size > 316.23 µm²
Filter on roundness (Polsby-Popper) > 0.6
density
size (µm²)
Quantify area of adipocytes
B
Frequency
log10 area in sq micro meters
subcutaneous
visceral
C
Adipocyte U-net 2-0 area
Adiposoft area per tile
regression
y=x
y=1.15x + −143.06
R2=0.76
D
Adipocyte U-net 2-0 area
Previous U−net area
regression
y=x
y=1.16x
R2=0.99

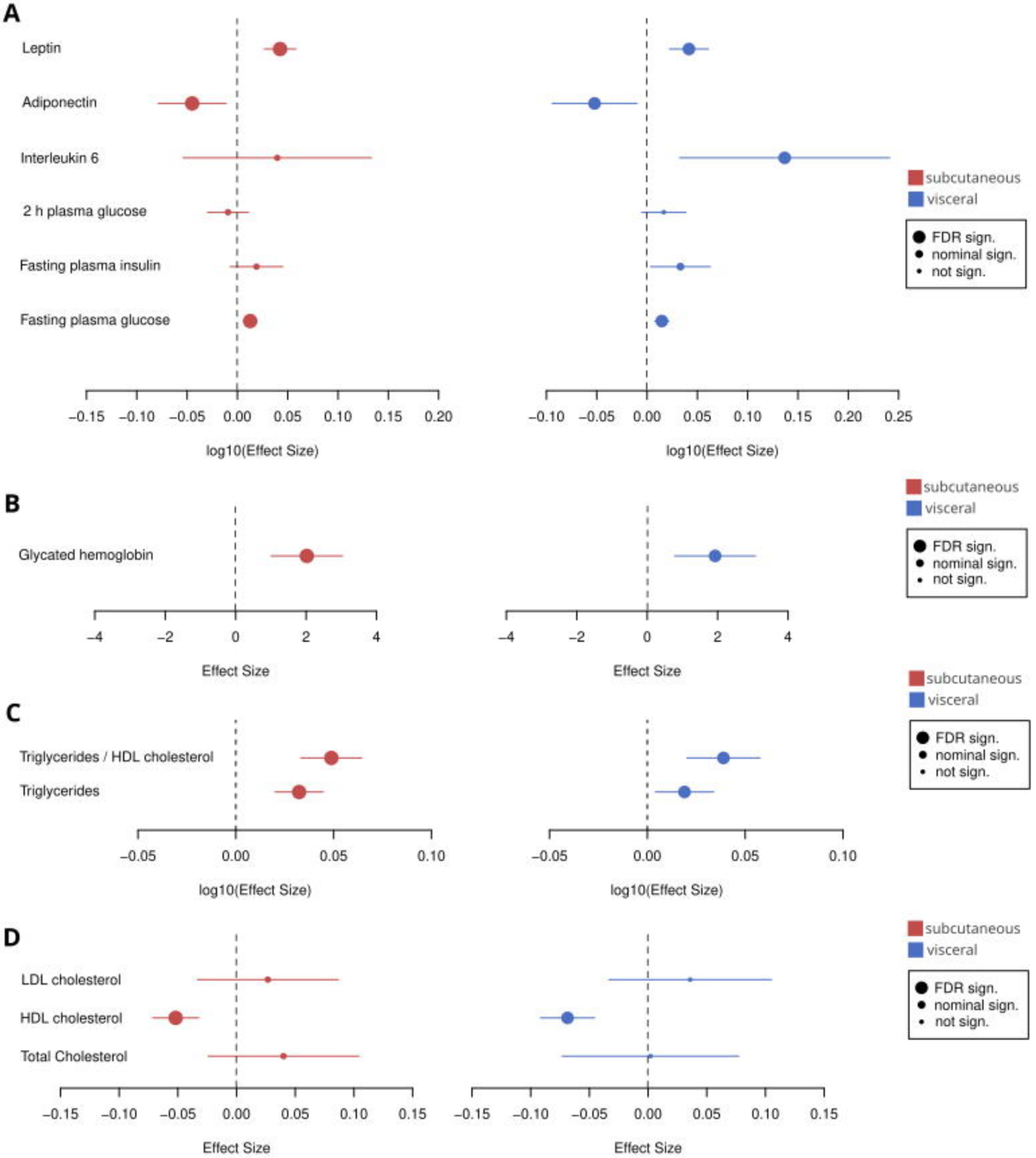
A
Leptin
Adiponectin
Interleukin 6
2 h plasma glucose
Fasting plasma insulin
Fasting plasma glucose
−0.15 −0.10 −0.05 0.00 0.05 0.10 0.15 0.20
log10(Effect Size)
−0.10 −0.05 0.00 0.05 0.10 0.15 0.20 0.25
log10(Effect Size)
subcutaneous
visceral
FDR sign.
nominal sign.
not sign.
B
Glycated hemoglobin
−4 −2 0 2 4
Effect Size
−4 −2 0 2 4
Effect Size
subcutaneous
visceral
FDR sign.
nominal sign.
not sign.
C
Triglycerides / HDL cholesterol
Triglycerides
−0.05 0.00 0.05 0.10
log10(Effect Size)
−0.05 0.00 0.05 0.10
log10(Effect Size)
subcutaneous
visceral
FDR sign.
nominal sign.
not sign.
D
LDL cholesterol
HDL cholesterol
Total Cholesterol
−0.15 −0.10 −0.05 0.00 0.05 0.10 0.15
Effect Size
−0.15 −0.10 −0.05 0.00 0.05 0.10 0.15
Effect Size
subcutaneous
visceral
FDR sign.
nominal sign.
not sign.

A

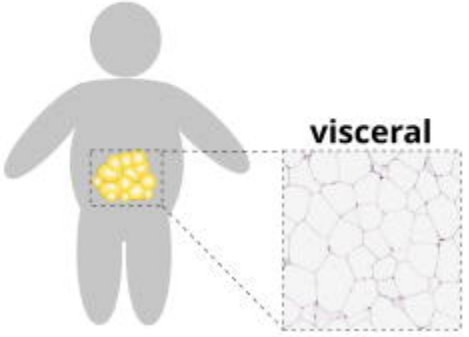

n = 1,878 individuals
95%-quantile adipocyte size

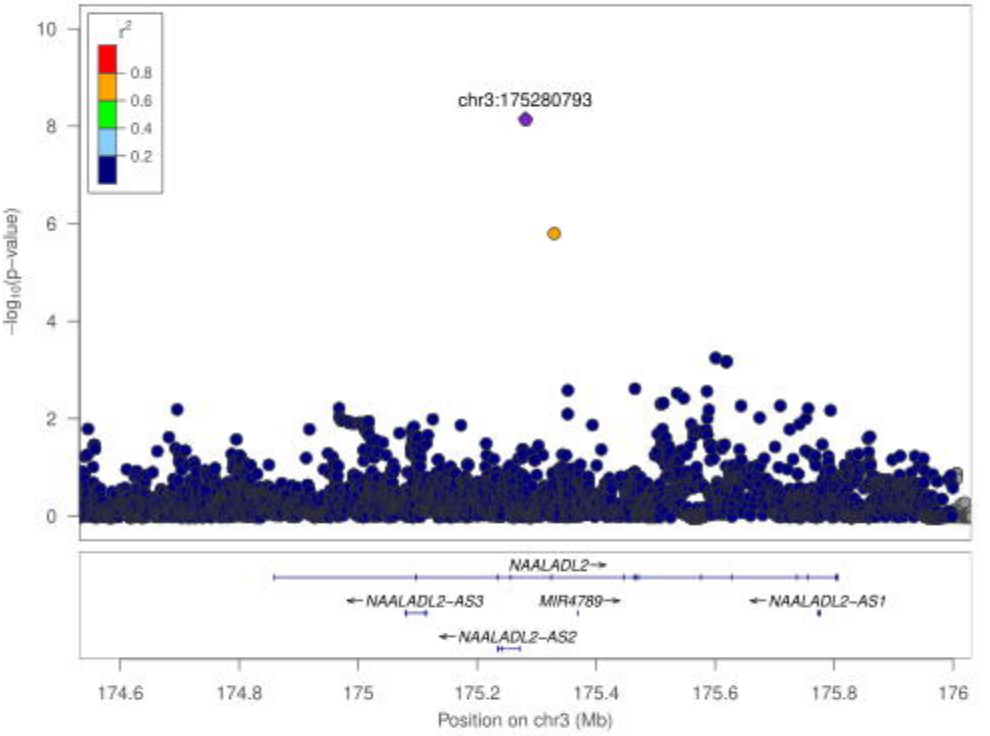

B

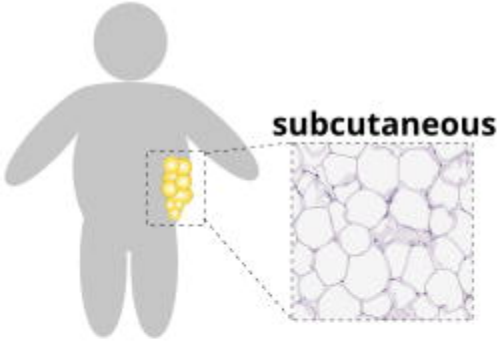
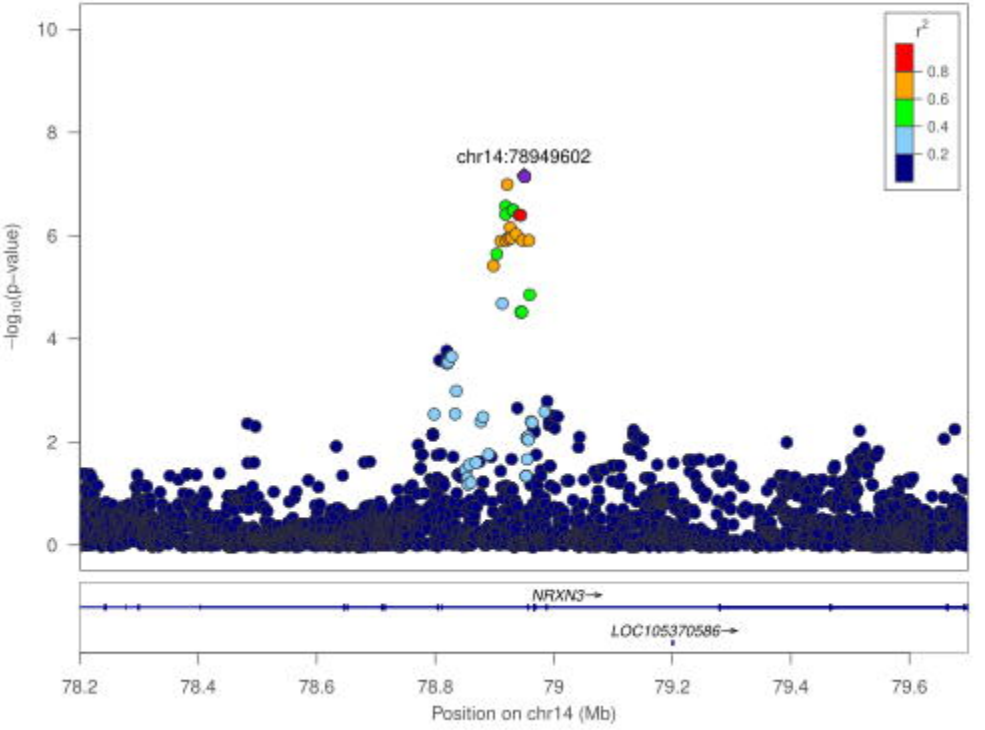
n = 2,066 individuals
95%-quantile adipocyte size